Observation of Magnetic State Dependent Thermoelectricity in Superconducting Spin Valves

César González-Ruano,[1] Diego Caso,[1] Jabir Ali Ouassou,[2] Coriolan Tiusan,[3,4] Yuan Lu,[4] Jacob Linder,[2] and Farkhad G. Aliev[5,*]

[1]*Departamento Física de la Materia Condensada C-III, Universidad Autónoma de Madrid, Madrid 28049, Spain*
[2]*Center for Quantum Spintronics, Department of Physics, Norwegian University of Science and Technology, NO-M7T9Q Trondheim, Norway*
[3]*Department of Solid State Physics and Advanced Technologies, Faculty of Physics, Babes-Bolyai University, Cluj Napoca 400114, Romania*
[4]*Institut Jean Lamour, Nancy Universitè, 54506 Vandoeuvre-les-Nancy Cedex, France*
[5]*Departamento Física de la Materia Condensada C-III, Instituto Nicolás Cabrera (INC) and Condensed Matter Physics Institute (IFIMAC), Universidad Autónoma de Madrid, Madrid 28049, Spain*

(Received 2 December 2022; revised 3 March 2023; accepted 8 May 2023; published 7 June 2023)

Superconductor-ferromagnet tunnel junctions demonstrate giant thermoelectric effects that are being exploited to engineer ultrasensitive terahertz radiation detectors. Here, we experimentally observe the recently predicted complete magnetic control over thermoelectric effects in a superconducting spin valve, including the dependence of its sign on the magnetic state of the spin valve. The description of the experimental results is improved by the introduction of an interfacial domain wall in the spin filter layer interfacing the superconductor. Surprisingly, the application of high in-plane magnetic fields induces a double sign inversion of the thermoelectric effect, which exhibits large values even at applied fields twice the superconducting critical field.

DOI: 10.1103/PhysRevLett.130.237001

Introduction.—The competition between superconductivity (S) and ferromagnetism (F) can under certain conditions result in a synergy of these otherwise antagonistic states [1]. In recent years, a variety of exotic phenomena have been demonstrated in devices that exploit this synergy. Notable examples include long-ranged spin-triplet supercurrents [2–4], spin-valve Josephson junctions [5], superconducting spin valves with record-high magnetoresistance, and the giant thermoelectric (TE) effect. These effects are considered as potential ingredients in the next generation of low-dissipation cryogenic devices [6–8].

In general, there exists considerable interest in identifying material platforms for improved TE devices. At low temperatures, TE effects are expected to be vanishingly small in both normal metals and bulk superconductors. Instead, they have been investigated mainly in superconductor/normal-metal hybrids, where they have been used in microrefrigeration and thermometry [9]. More recently, fascinating theoretical predictions [10–15] have opened the door to unexplored spin-dependent TE effects in S/F hybrids. The transport of spin and charge due to temperature gradients in such systems have only been investigated experimentally in a few works [16–19]. Kolenda *et al.* [16] reported on the experimental observation of an enhanced Seebeck coefficient (up to 100 $\mu V/K$) when a large magnetic field of 1 T splits the quasiparticle band structure of a superconductor. When combined with a spin-filtering interface, this spin splitting breaks the electron-hole symmetry, producing the observed "giant TE effect" that is now being exploited to develop ultrasensitive radiation detectors [20].

So far, the experimental tuning of giant TE effects in S/F hybrids has been performed either by applying large magnetic fields [16] or by exchange coupling a superconductor to a ferromagnetic insulator [20]. Recently, however, a different method to control the TE effect has been predicted in superconductor/ferromagnet/ferromagnetic insulator systems [21]. This method can turn the superconducting TE effect on and off *in situ*, as well as reversing its sign. Here, by interfacing a superconductor with a spin valve with large spin filtering capability, we experimentally demonstrate the mentioned complete magnetic control of the superconducting TE effect. This includes evidence of an antisymmetric TE effect, where a change of the magnetic state of the spin valve inverts the direction of the TE current. Controlling the sign of the thermopower, analogous to the inversion of TE signals between p- and n-doped semiconductors, enables the design of Peltier elements based on superconducting spin valves.

Experimental results.—Figure 1(a) illustrates the main experimental setup and junctions investigated. We have measured TE effects in V(40)/MgO(2)/Fe(10)/MgO(2)/Fe(10)/Co(20) single-crystalline junctions epitaxially grown

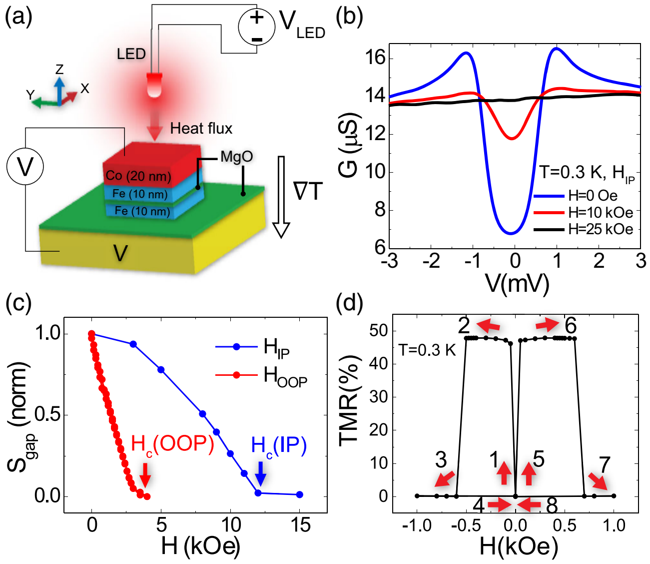

FIG. 1. (a) Sketch of the $S/F/F$ junctions when heated by a LED. (b) Typical conductance-bias curves measured at $0.07T_c$ at three different applied IP magnetic fields. (c) Normalized superconducting gap depth (S_{gap}) taken from $G(V)$ curves vs applied IP and OOP magnetic fields. (d) Typical tunneling magnetoresistance (TMR) curves measured with IP magnetic field at $V = 5$ mV and $T = 0.3$ K. The numbers indicate the order of the field sweeping and resistance changes.

on MgO(001) substrates, with the thickness of each layer given in nanometers in parentheses. More details about the junctions, experimental setup, and procedures can be found in the Supplemental Material [22]. Here, V is a BCS superconductor, Fe and Co are ferromagnetic metals, and MgO is a symmetry filtering insulator. The magnetically hard Fe-Co electrode allows a precise detection of the orientation of the magnetically free Fe layer interfacing the superconductor. Figures 1(b) and 1(c) present a general electron transport characterization of the junctions in the superconducting state as a function of the applied bias and external magnetic field. The superconducting gap in the V electrode is suppressed by in-plane (IP) and out-of-plane (OOP) fields of about 1.7 T and 0.4 T, respectively [Fig. 1(c)]. The magnetoresistance values of 35%–55% provide an estimation of the effective spin polarization of the Fe electrodes of around 0.75–0.85 for the different junctions studied based on the Slonczewski model, which was adapted for the case of two resistances in series, one of which depends on the relative magnetization angle and spin polarization. This procedure and results are line with previous reports [31,32]. At first glance, these tunneling magnetoresistance (TMR) values of ~45% may seem very low compared to crystalline F/F junctions where values from 180% to 300% have been reported [33,34]. However, this value is not related to the quality of the crystalline structure [note for example the polarization values in Fig. 4(b), exceeding 0.8], but rather with the fact that the structure of these junctions is $N/F/F$, including a normal metal electrode (vanadium) with a second tunnel barrier, which has an almost fixed resistance and strongly hampers the total TMR ratio. Indeed, in experiments in control F/F junctions grown in the same conditions, we have previously observed TMR values from 185% to 330% [35,36]. Further evidence for the high crystalline quality and effective spin filtering in our V/MgO/Fe/MgO/Fe/Co junctions comes from their record high tunneling magnetoresistance achieved at biases exceeding 1 V [36].

To study the TE effect as a function of the spin-valve state, the soft Fe layer was rotated while the hard Fe-Co layer remained fixed. We did this by applying a rotating in-plane magnetic field, with a magnitude between the coercive fields of the two magnetic layers. For the hard layer the coercive field is typically larger than 500 Oe [Fig. 1(d)], while for the soft layer it is smaller than 50 Oe, determined by the magnetocrystalline anisotropy. This procedure guarantees a reorientation between the parallel (P), antiparallel (AP), and perpendicular in-plane (PIP) configurations of the spin valve. For each 3° rotation of the applied field, the temperature gradient ∇T was re-established via the LED heater, and the resulting TE response ΔV was measured.

Figure 2(a) shows the variation of the TE voltage generated during a magnetization rotation of the free layer under an in-plane applied magnetic field of 70 Oe. While the transition between the P and PIP states hardly affects the values of the TE response, a strong reduction of the TE voltage of more than a factor of 2 is observed when the free layer becomes close to AP to the fixed Fe-Co layer. Note that there is a slight latency of about 10°–15° between the angle of the applied magnetic field and the real average magnetization orientation of the Fe layer. This is a natural consequence of the experimental process: the Fe magnetization has to overcome the magnetocrystalline anisotropy to follow the slowly rotating applied field (see, for example, Ref. [37]). The complete 360° rotation takes about 2 h, since we stop at each intermediate angle to measure the TE response. Figures 2(b) and 2(c) show the TE response of the samples vs the induced temperature gradient for different magnetic configurations and applied fields. Note that these temperature gradients have been estimated by first simulating the response to the incoming heat flux and subsequently recalculating ΔT from V_{LED} based on the LED calibration curves (see Supplemental Material [22]). In the P state, changing the applied field by less than a few hundred Oe does not qualitatively change the TE response [Fig. 2(b)]. However, in the AP state, varying the magnetic field has a dramatic effect on the TE response and can even change its sign as seen in Fig. 2(c). We note that no asymmetry of ΔV or dependence on V_{LED} was observed above T_c [Fig. 2(a)]. Control experiments on short-circuited junctions also revealed at least an order of magnitude drop of the TE response regardless of the magnetic state (see Supplemental Material [22]).

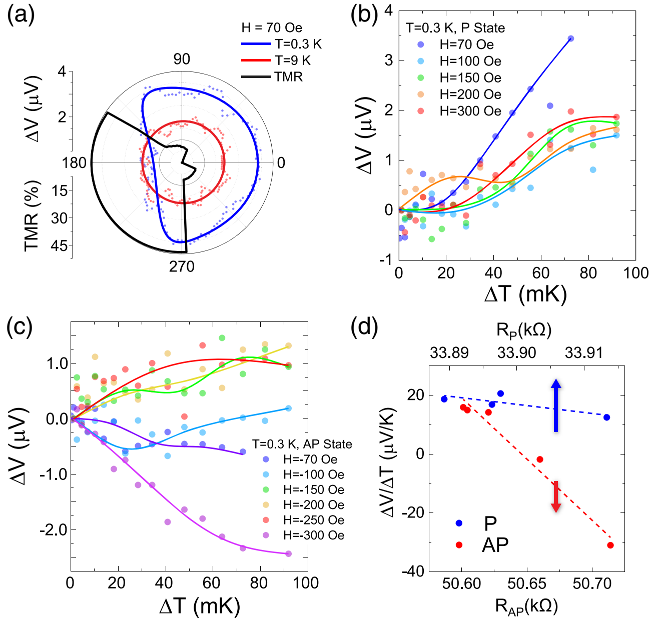

FIG. 2. Thermoelectric response of a $S/F/F$ junction measured under a rotation and fixed values of the applied magnetic field at $T = 0.3$ K. (a) TE response at $H = 70$ Oe for in-plane rotations of the magnetic field at $V_{\mathrm{LED}} = 7.3$ V ($\Delta T \approx 113$ mK), below and above T_c. The tunnel magnetoresistance of the spin valve is also displayed against the rotation angle. (b) Response in the P configuration of the spin-valve stack. (c) Same experiment for the AP configuration. The TE voltage changes its sign and intensity depending not directly on the applied field, but on the saturation of the soft F layer. The related analysis is shown in panel (d), where the average value of the TE voltage is plotted against the measured resistance for the P (blue, upper horizontal axis) and AP (red, lower horizontal axis) configurations. For the P state, a lower resistance implies a better polarization, while in the AP state the polarization is better with a higher resistance.

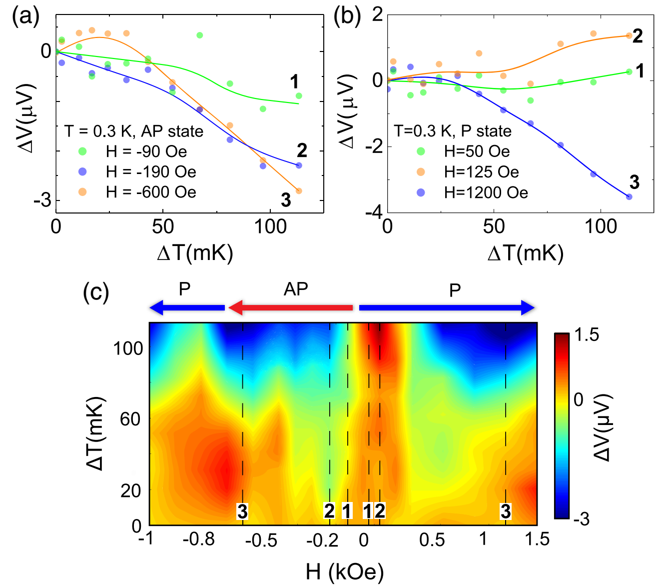

FIG. 3. Thermoelectric voltage of an $S/F/F$ junction demonstrating sign inversion at high fields in the AP state (a) and P state (b). (c) Color map of the recorded TE voltage ΔV as a function of the temperature difference ΔT and the applied in-plane field H for the same junction, indicating the P and AP states.

In order to understand the possible reasons for the TE sign change in the AP state, we analyzed [Fig. 2(d)] the TE response obtained for a fixed temperature gradient as a function of the resistance in the P and AP states obtained during each particular TE experiment at different applied in-plane magnetic fields (not exceeding 500 Oe). While the TE response in the P state is rather robust to the variation of the resistance (i.e., presence of magnetic inhomogeneities), in the AP state it changes sign with the *reduction* of the influence of these magnetic textures (an increase of the resistance means better magnetization saturation).

Interestingly, some junctions revealed a TE sign inversion both in the AP state and also under a sufficiently high applied in-plane magnetic field in the P state (Fig. 3). The TE response in the P state is positive and robust at fields below 0.5 kOe [Fig. 3(a)], and becomes negative for higher magnetic fields. In contrast, in the AP state the TE response is already negative for much smaller fields [Fig. 3(b)], right after the spin valve switched into the AP state [see steps 1 and 2 in Fig. 1(d)]. Further increasing the negative magnetic field [paths 2 and 3 in Fig. 1(d)] reorients the hard layer so the spin valve is again in the P configuration, and again the sign of the TE effect follows the same trend as for positive fields. Figure 3(c) summarizes these observations with a 3D color plot of the TE voltage signal against the applied field and evaluated temperature gradient. Figure 3(a) also shows that ΔV could change sign as a function of ΔT at fixed magnetic field H. One potential explanation could be a temperature-induced change in the interfacial domain wall structure, as discussed in the Supplemental Material [22].

We have found that the TE voltage sign inversion in the P state under high in-plane magnetic fields is a rather robust effect and is followed by a second TE sign inversion toward positive values when the magnetic field is further increased [Fig. 4(a)]. Surprisingly, even for maximum applied in-plane magnetic fields, twice exceeding the second critical magnetic field [compare Fig. 1(c) and Fig. 4(a)], the TE voltage remains high and without clear signatures of diminishing. A qualitatively similar response has been observed in single barrier V/MgO/Fe junctions, i.e. without the sensing Fe/Co layer. Figure 4(b) compares the TE signal inversion field with the TMR and effective spin polarization values of each corresponding sample. Apparently, a higher TMR and correspondingly polarization values shift the TE inversion field range outside our experimental capabilities (35 kOe). This suggests a possible link between the observed effect and interfacial domain wall forming in the Fe electrode. Further experiments are needed to understand the physical mechanism behind the high field TE effects.

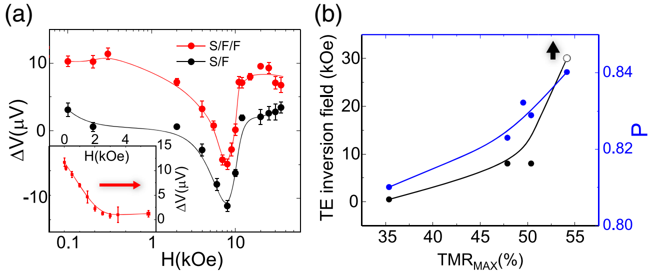

FIG. 4. (a) Thermoelectric voltage of an $S/F/F$ and S/F junction at $V_{\mathrm{LED}} = 7.3$ V ($\Delta T \approx 113$ mK) vs applied in-plane field at $T = 0.3$ K. The high-field sign inversion is achieved in both samples, and the TE effect is maintained with increasing in-plane fields up to 30 kOe. The inset displays the measured TE voltage in the $S/F/F$ junction under out-of-plane field. At $H = H_c$, superconductivity and its associated TE voltage vanish. (b) TE inversion field and polarization against the maximum TMR value for all the $S/F/F$ junctions under study.

Theoretical modeling.—To better understand the physics behind the experimental observations, we explored the setup in Fig. 1(a) via numerical simulations. We employed the Usadel formalism [38–42], which describes superconductivity in diffusive heterostructures, together with spin-dependent tunneling boundary conditions [10,43–46] valid for arbitrary spin polarizations. To numerically solve these equations, we used the Ricatti parameterization [47,48] to calculate spectral properties and a distribution-trace parameterization [40–42,49] to calculate the nonequilibrium transport properties. The theoretical and numerical approaches are described in more detail in Ref. [21].

The numerical model used herein is sketched in Fig. 5(a). The superconductor (V) was treated as a BCS superconducting reservoir with an effective spin-splitting $h = \Delta/10$, near-zero temperature $T = T_c/100$, and electrical grounding $V = 0$. The hard ferromagnet (Fe-Co) was treated as a nonsuperconducting metallic reservoir at an elevated temperature $T = T_c/2$ and voltage $V = \Delta V$. The interfaces to the soft ferromagnet (V-MgO-Fe and Fe-MgO-Fe-Co) were treated using spin-polarized tunneling boundary conditions with spin polarizations P_1, P_2 and a low tunneling conductance $G_T = G_D/5$, where G_D is the Drude conductance of the soft ferromagnet. These parameters model the high spin filtering capabilities and low transparencies of the MgO barriers. In the soft ferromagnet (Fe), we used an exchange splitting $h = 30\Delta$. For each magnetic configuration, we (i) solved the Usadel equation for 80 different $e\Delta V/\Delta \in [-0.04, +0.04]$, (ii) used this to calculate the current $I(\Delta V)$, and (iii) interpolated the open-circuit voltage from $I(\Delta V) \equiv 0$. This yielded the TE voltage as function of magnetic configuration.

The magnetic configurations we considered are illustrated in Figs. 5(a) and 5(b). We take the hard ferromagnet (red) to be oriented along one in-plane axis (up), and the spin filtering at the MgO barrier is assumed to be parallel to this orientation (black). The soft ferromagnet is then rotated

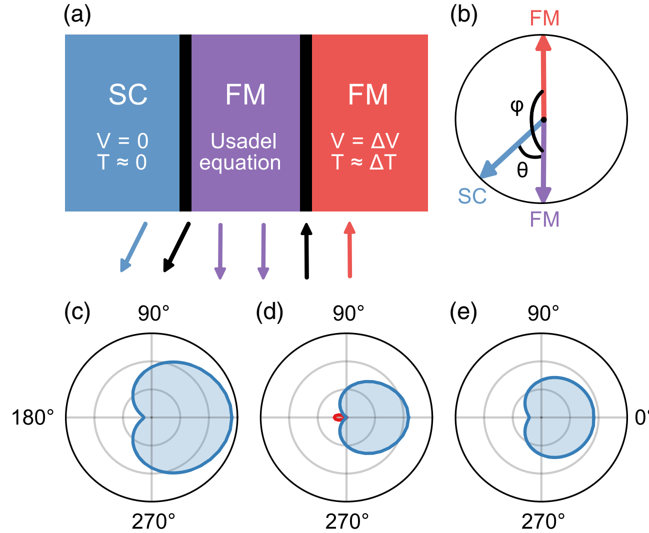

FIG. 5. (a) Sketch of the system modelled, with the superconducting (SC) and ferromagnetic (FM) layers indicating the relevant values and calculations used in each one. (b) Definitions of angles θ and φ with respect to the field directions in the model. (c)–(e) Numerical results for the magnetically dependent thermoelectric voltage $\Delta V(\varphi)$. Blue and red correspond to positive and negative voltages, while the radius in each plot is $|\Delta V| = 0.04\Delta/e$ where e is the elementary charge. The three plots correspond to (c) $\theta = 0$, $P_1 = P_2 = 80\%$; (d) $\theta = 0$, $P_1 = 60\%$, $P_2 = 80\%$; (e) $\theta = \pi/4$, $P_1 = 60\%$, $P_2 = 80\%$.

by an in-plane angle φ relative to the hard ferromagnet (purple), which here is sketched for the antiparallel case $\varphi = \pi$. At the superconductor interface, we include the possibility for an interfacial domain wall described by an out-of-plane angle θ. This affects both the spin filtering at the second MgO barrier (black) and the direction of spin splitting inside the neighboring superconductor (blue). Figures 5(c)–5(e) show the numerical results for the TE voltage $\Delta V(\varphi)$ across the junction as function of the in-plane misalignment angle between the two ferromagnets. In panel (c), we see the predicted response for a junction with two identical spin filters ($P_1 = P_2$) and no interfacial domain wall ($\theta = 0$). We then predict an *asymmetric TE effect*, by which we mean that $\Delta V(0)$ is maximal while $\Delta V(\pi) \to 0$. This can be understood intuitively as follows. If the two spin filters are identical ($P_1 = P_2$ and $\varphi = 0$), then “filtering the spins twice” does not significantly change the physics compared to having only one spin filter. The latter case has in previous work been shown to produce a giant TE effect in superconductor-ferromagnet systems [10–19]. On the other hand, the effects of two identical but oppositely aligned spin filters cancel, so any TE effect due to spin filtering should vanish for $\varphi = \pi$. In panel (d), we see the case of different spin filters ($P_1 < P_2$). It is now possible for one ferromagnet to dominate the spin splitting of the superconducting density of states, while the other dominates the spin filtering process. Via the mechanism explored in detail in [21], this leads to an antisymmetric contribution to $\Delta V(\varphi)$, whereby $\Delta V(0)$ and $\Delta V(\pi)$ have opposite signs. In the extreme case of $P_1 \ll P_2$, the result is a purely antisymmetric shape for $\Delta V(\varphi)$, whereas for P_1, P_2 of similar magnitude the theory predicts $|\Delta V(\pi)| \ll |\Delta V(0)|$. In panel (e), we show the effect of adding an out-of-plane interfacial domain wall to panel (d), which clearly suppresses the antisymmetric contribution.

While the simplest model presented in Fig. 5(c) captures the essential features of Fig. 2(a), including an interfacial domain wall in the model enhances the agreement with the experiment. Specifically, in the absence of externally applied fields, such a domain wall would produce the results in panel Fig. 5(e), which also agree well with Fig. 2(a). However, as the in-plane applied field is ramped up, the domain wall should be rotated into the thin-film plane: $\theta \to 0$. In this case, we would gradually move toward panel (d), where $\Delta V(\varphi)$ changes sign. This qualitatively agrees with the experimental observations in Fig. 2(d), where it is found that $\Delta V(\pi)$ changes sign for increasing magnetic saturation while $\Delta V(0)$ changes only slightly. For plots of ΔV as a function of θ, thus modeling the magnetic field dependence of the thermoelectric effect, see the Supplemental Material [22].

Discussion and conclusions.—While our numerical modeling qualitatively explains the experiments at low magnetic fields where the switching between the P and AP states takes place (Figs. 2, 3, and 5), it does not account for the unexpected strong variation of the TE response in the high-field limit, where a double sign change takes place regardless of the presence of the magnetically hard layer (Fig. 4). This is because the spin-resolved particle-hole asymmetry in quasiclassical theory is only present in the superconducting state. A possible factor that may influence the high-field TE response is a transformation of the interfacial magnetism at the V-MgO interface [50] under an applied magnetic field. Initially predicted by numerical simulations [51], spin fluctuations and/or surface atomic layer magnetism in V have been under debate for decades now [52–56]. In our experiments, a sufficiently large in-plane magnetic field could transform the V-MgO interface into an additional, atomically thin magnetic layer. The induced surface magnetism might strongly affect the exchange splitting of the electron bands in V. The explanation of the high-field TE response behavior remains an intriguing open problem.

In conclusion, we report on the experimental control of the superconducting thermoelectric effect using a spin-valve device with a spin filter. We demonstrate both experimentally and by numerical simulations the transition from a strongly asymmetric to an antisymmetric response depending on the saturation of the AP alignment of the spin valve, which is likely modulated by an interfacial domain wall. Furthermore, our results point toward an unexpected thermoelectric response in superconductor-ferromagnet junctions under high in-plane magnetic fields. More detailed experimental and theoretical studies are required to understand this behavior.

Authors thank Michel Hehn for discussions and help with samples preparation. The work in Madrid was supported by Spanish Ministry of Science and Innovation (PID2021-124585NB-C32 and TED2021-130196B-C22) and Consejería de Educación e Investigación de la Comunidad de Madrid (NANOMAGCOST-CM Ref. P2018/NMT-4321) Grants. F. G. A. also acknowledges financial support from the Spanish Ministry of Science and Innovation through the María de Maeztu Programme for Units of Excellence in R&D (CEX2018-000805-M) and “Acción financiada por la Comunidad de Madrid en el marco del convenio plurianual con la Universidad Autónoma de Madrid en Línea 3: Excelencia para el Profesorado Universitario.” The work in Trondheim was supported by the Research Council of Norway through Grant No. 323766, and its Centres of Excellence funding scheme Grant No. 262633 “QuSpin”. J. L. and J. A. O. also acknowledge resources provided by Sigma2—the National Infrastructure for High Performance Computing and Data Storage in Norway. C. T. acknowledges the UEFISCDI project “MODESKY”ID PN-III-P4-ID-880 PCE-2020-0230-P, Grant No. UEFISCDI: PCE 245/02.11.2021.

C. G.-R. and D. C. contributed equally to the work.

*Corresponding author.
farkhad.aliev@uam.es

[1] A. I. Buzdin, Proximity effects in superconductor-ferromagnet heterostructures, Rev. Mod. Phys. **77**, 935 (2005).

[2] R. S. Keizer, S. T. B. Goennenwein, T. M. Klapwijk, G. Miao, G. Xiao, and A. Gupta, A spin triplet supercurrent through the half-metallic ferromagnet CrO_2, Nature (London) **439**, 825 (2006).

[3] J. W. A. Robinson, J. D. S. Witt, and M. G. Blamire, Controlled injection of spin-triplet supercurrents into a strong ferromagnet, Science **329**, 59 (2010).

[4] Trupti S. Khaire, Mazin A. Khasawneh, W. P. Pratt, Jr., and Norman O. Birge, Observation of Spin-Triplet Superconductivity in Co-Based Josephson Junctions, Phys. Rev. Lett. **104**, 137002 (2010).

[5] B. M. Niedzielski, T. J. Bertus, J. A. Glick, R. Loloee, W. P. Pratt, Jr., and N. O. Birge, Spin-valve Josephson junctions for cryogenic memory, Phys. Rev. B **97**, 024517 (2018).

[6] G. Yang, C. Ciccarelli, and J. W. A. Robinson, Boosting spintronics with superconductivity, APL Mater. **9**, 050703 (2021).

[7] A. E. Madden, J. C. Willard, R. Loloee, and N. O. Birge, Phase controllable Josephson junctions for cryogenic memory, Supercond. Sci. Technol. **32**, 015001 (2018).

[8] L. Ai, E. Zhang *et al.*, Van der Waals ferromagnetic Josephson junctions, Nat. Commun. **12**, 6580 (2021).

[9] F. Giazotto, T. T. Heikkilä, A. Luukanen, A. M. Savin, and J. P. Pekola, Opportunities for mesoscopics in thermometry

and refrigeration: Physics and applications, Rev. Mod. Phys. **78**, 217 (2009).

[10] P. Machon, M. Eschrig, and W. Belzig, Nonlocal Thermoelectric Effects and Nonlocal Onsager relations in a Three-Terminal Proximity-Coupled Superconductor-Ferromagnet Device, Phys. Rev. Lett. **110**, 047002 (2013).

[11] P. Machon, M. Eschrig, and W. Belzig, Giant thermoelectric effects in a proximity-coupled superconductor–ferromagnet device, New J. Phys. **16**, 073002 (2014).

[12] A. Ozaeta, P. Virtanen, F. S. Bergeret, and T. T. Heikkila, Predicted Very Large Thermoelectric Effect in Ferromagnet-Superconductor Junctions in the Presence of a Spin-Splitting Magnetic Field, Phys. Rev. Lett. **112**, 057001 (2014).

[13] M. S. Kalenkov and A. D. Zaikin, Electron-hole imbalance and large thermoelectric effect in superconducting hybrids with spin-active interfaces, Phys. Rev. B **90**, 134502 (2014).

[14] P. Dutta, A. Saha, and A. M. Jayannavar, Thermoelectric properties of a ferromagnet-superconductor hybrid junction: Role of interfacial Rashba spin-orbit interaction, Phys. Rev. B **96**, 115404 (2017).

[15] T. Savander, S. Tamura, C. Flindt, Y. Tanaka, and P. Burset, Thermoelectric detection of Andreev states in unconventional superconductors, Phys. Rev. Res. **2**, 043388 (2020).

[16] S. Kolenda, M. J. Wolf, and D. Beckmann, Observation of Thermoelectric Currents in High-Field Superconductor-Ferromagnet Tunnel Junctions, Phys. Rev. Lett. **116**, 097001 (2016).

[17] S. Kolenda, P. Machon, D. Beckmann, and W. Belzig, Nonlinear thermoelectric effects in high-field superconductor-ferromagnet tunnel junctions, J. Nanosci. Nanotechnol. **7**, 1579 (2016).

[18] S. Kolenda, C. Surgers, G. Fischer, and D. Beckmann, Thermoelectric effects in superconductor-ferromagnet tunnel junctions on europium sulfide, Phys. Rev. B **95**, 224505 (2017).

[19] J. Heidrich and D. Beckmann, Nonlocal thermoelectric effects in high-field superconductor-ferromagnet hybrid structures, Phys. Rev. B **100**, 134501 (2019).

[20] T. T. Heikkila, R. Ojajarvi, I. J. Maasilta, E. Strambini, F. Giazotto, and F. S. Bergeret, Thermoelectric Radiation Detector Based on Superconductor-Ferromagnet Systems, Phys. Rev. Appl. **10**, 034053 (2018).

[21] J. A. Ouassou, C. González-Ruano, D. Caso, F. G. Aliev, and J. Linder, Complete magnetic control over the superconducting thermoelectric effect, Phys. Rev. B **106**, 094514 (2022).

[22] See Supplemental Material at http://link.aps.org/supplemental/10.1103/PhysRevLett.130.237001, which includes Refs [23–30], for the experimental and samples setup, the modeling of the temperature profile via simulations, and the control measurement of the thermoelectric response in a short-circuited $S/F/F$.

[23] COMSOL Multiphysics® www.comsol.com. COMSOL AB, Stockholm, Sweden.

[24] M. Dixon, F. E. Hoare, T. M. Holden, and D. E. Moody, The low temperature specific heats of some pure metals (Cu, Ag, Pt, Al, Ni Fe Co), Proc. R. Soc. A **285**, 561 (1965).

[25] J. W. Gardner and A. C. Anderson, Effect of neutron irradiation on the low-temperature specific heat and thermal conductivity of magnesium oxide, Phys. Rev. B **23**, 415 (1981).

[26] Wayne Douglas Jung, The thermal conductivity of high purity vanadium, Retrospective Theses and Dissertations. Paper 5485 (1975), https://citeseerx.ist. psu.edu/document?repid=rep1&type=pdf&doi=d00eaf42ee3b96d1081d549b23cb9b28ca742066.

[27] R. Radebaugh and P. H. Keesom, Low-temperature thermodynamic properties of vanadium, Phys. Rev. **149**, 19 (1966).

[28] M. Walter, J. Walowski, V. Zbarsky, M. Munzenberg, M. Schafers, D. Ebke, G. Reiss, A. Thomas, P. Peretzki, M. Seibt, J. S. Moodera, M. Czerner, M. Bachmann, and C. Heiliger, Seebeck effect in magnetic tunnel junctions, Nat. Mater. **10**, 742 (2011).

[29] C. Tiusan, M. Hehn, F. Montaigne, F. Greullet, S. Andrieu, and A. Schuhl, Spin tunneling phenomena in single crystal magnetic tunnel junction systems, J. Phys. Condens. Matter **19**, 165201 (2007).

[30] C. González-Ruano, D. Caso, L. G. Johnsen, C. Tiusan, M. Hehn, N. Banerjee, J. Linder, and Farkhad G. Aliev, Superconductivity assisted change of the perpendicular magnetic anisotropy in V/MgO/Fe junctions, Sci. Rep. **11**, 19041 (2021).

[31] I. Martínez, C. Tiusan, M. Hehn, M. Chshiev, and F. G. Aliev, Symmetry broken spin reorientation transition in epitaxial MgO/Fe/MgO layers with competing anisotropies, Sci. Rep. **8**, 9463 (2018).

[32] C. González-Ruano, L. G. Johnsen, D. Caso, C. Tiusan, M. Hehn, N. Banerjee, J. Linder, and F. G. Aliev, Superconductivity-induced change in magnetic anisotropy in epitaxial ferromagnet-superconductor hybrids with spin-orbit interaction, Phys. Rev. B **102**, 020405(R) (2020).

[33] S. Parkin, C. Kaiser, A. Panchula, P. M. Rice, B. Hughes, M. Samant, and S.-H. Yang, Giant tunnelling magnetoresistance at room temperature with MgO (100) tunnel barriers, Nat. Mater. **3**, 862 (2004).

[34] S. Yuasa, T. Nagahama, A. Fukushima, Y. Suzuki, and K. Ando, Giant room-temperature magnetoresistance in single-crystal Fe/MgO/Fe magnetic tunnel junctions, Nat. Mater. **3**, 868 (2004).

[35] R. Guerrero, D. Herranz, and F. G. Aliev, High bias voltage effect on spin-dependent conductivity and shot noise in carbon-doped Fe(001)/MgO(001)/Fe(001) magnetic tunnel junctions, Appl. Phys. Lett. **91**, 132504 (2007).

[36] C. González-Ruano, C. Tiusan, M. Hehn, and F. G. Aliev, Boosting room temperature tunnel magnetoresistance in hybrid magnetic tunnel junctions under electric bias, Adv. Electron. Mater. **8**, 2100805 (2021).

[37] M. S. Gabor, T. Petrisor, Jr., C. Tiusan, M. Hehn, and T. Petrisor, Magnetic and structural anisotropies of Co_2FeAl Heusler alloy epitaxial thin films, Phys. Rev. B **84**, 134413 (2011).

[38] K. D. Usadel, Generalized Diffusion Equation for Superconducting Alloys, Phys. Rev. Lett. **25**, 507 (1970).

[39] J. Rammer and H. Smith, Quantum field-theoretical methods in transport theory of metals, Rev. Mod. Phys. **58**, 323 (1986).

[40] F. S. Bergeret, M. Silaev, P. Virtanen, and T. T. Heikkilä, Colloquium: Nonequilibrium effects in superconductors with a spin-splitting field, Rev. Mod. Phys. **90**, 041001 (2018).

[41] V. Chandrasekhar, *Superconductivity*, edited by K. Bennemann and J. Ketterson (Springer, Berlin, 2008).

[42] W. Belzig, F. K. Wilhelm, C. Bruder, G. Schön, and A. D. Zaikin, Quasiclassical Green's function approach to mesoscopic superconductivity, Superlattices Microstruct. **25**, 1251 (1999).

[43] J. A. Ouassou, A. Pal, M. Blamire, M. Eschrig, and J. Linder, Triplet Cooper pairs induced in diffusive s-wave superconductors interfaced with strongly spin-polarized magnetic insulators or half-metallic ferromagnets, Sci. Rep. **7**, 1932 (2017).

[44] M. Eschrig, A. Cottet, W. Belzig, and J. Linder, General boundary conditions for quasiclassical theory of superconductivity in the diffusive limit: Application to strongly spin-polarized systems, New J. Phys. **17**, 083037 (2015).

[45] A. Cottet, D. Huertas-Hernando, W. Belzig, and Y. V. Nazarov, Spin-dependent boundary conditions for isotropic superconducting Green's functions, Phys. Rev. B **80**, 184511 (2009).

[46] A. Cottet, Spectroscopy and critical temperature of diffusive superconducting/ferromagnetic hybrid structures with spin-active interfaces, Phys. Rev. B **76**, 224505 (2007).

[47] S. H. Jacobsen, J. A. Ouassou, and J. Linder, Critical temperature and tunneling spectroscopy of superconductor-ferromagnet hybrids with intrinsic Rashba-Dresselhaus spin-orbit coupling, Phys. Rev. B **92**, 024510 (2015).

[48] N. Schopohl, Transformation of the Eilenberger equations of superconductivity to a scalar Riccati equation (unpublished).

[49] J. A. Ouassou, T. D. Vethaak, and J. Linder, Voltage-induced thin-film superconductivity in high magnetic fields, Phys. Rev. B **98**, 144509 (2018).

[50] C. Rau, C. Liu, A. Schmalzbauer, and G. Xing, Ferromagnetic Order at (100) $p(1 \times 1)$ Surfaces of Bulk Paramagnetic Vanadium, Phys. Rev. Lett. **57**, 2311 (1986).

[51] D. R. Grempel and S. C. Ying, Spin Fluctuations at the Surface of Vanadium, Phys. Rev. Lett. **45**, 1018 (1980).

[52] T. G. Walker and H. Hopster, Induced magnetic order in ultrathin vanadium films on Fe(100), Phys. Rev. B **49**, 7687 (1994).

[53] P. Fuchs, K. Totland, and M. Landolt, Induced magnetization in thin epitaxial V films on Fe(100), Phys. Rev. B **53**, 9123 (1996).

[54] T. Bryk, D. M. Bylander, and L. Kleinman, Magnetism of the V(001) surface in the generalized gradient approximation, Phys. Rev. B **61**, R3780(R) (2000).

[55] D. Lacina, J. Yang, and J. L. Erskine, Multilayer relaxation and search for ferromagnetic order at the (100) surface of bulk paramagnetic vanadium, Phys. Rev. B **75**, 195423 (2007).

[56] A. Rubio-Ponce, D. Olguín, A. Aguayo, and R. de Coss, Surface magnetism in vanadium overlayers on W(100), J. Magn. Magn. Mater. **514**, 167143 (2020).